Chalcogenide Glasses ☆

K Tanaka, Hokkaido University, Sapporo, Japan

A chalcogenide glass is the one containing a large amount of chalcogen atoms, sulfur, selenium, and tellurium. More widely, oxide glasses may be included in this category, but they are treated as references in the present article. A variety of stable chalcogenide glasses such as Se, $As_2S(Se)_3$, $Ge_2Sb_2Te_5$, etc. can be prepared in bulk, fiber, thin film, and multilayer forms using melt-quenching, vacuum deposition, and other less common techniques.

The atomic bonding structure is, in general, more rigid than that of organic polymers and more flexible than that of oxide glasses. Accordingly, the glass-transition temperatures and elastic properties lie in between those of these materials. Some chalcogenide glasses containing silver such as $AgAsS_2$ and so forth behave as (super-)ionic conductors.

As demonstrated by Kolomiets around 1950, these glasses behave as semiconductors or, more strictly, they are a kind of amorphous semiconductor with bandgap energies of 1–3 eV. Electronic properties, which are governed by the species of chalcogen atoms, are modified by disordered structures, while the relationship between the structure and electronic properties remains to be studied.

Since several books have provided reviews on the chalcogenide glass from standpoints of non-crystalline materials (Mott and Davis, 1979; Elliott, 1990), amorphous semiconductors (Popescu, 2000; Singh and Shimakawa, 2003; Tanaka and Shimakawa, 2011), and glasses (Borisova, 1981; Elliott, 1991; Kokorina, 1996; Fairman and Ushkov, 2004; Wang, 2014; Adam and Zhang, 2014), this section attempts to be an introduction to those publications, mainly emphasizing the nature of chalcogenide glasses in comparison with other materials. In addition, new insights, remaining problems, and applications are properly referred to wherever possible.

1 Structural

Glass formation of chalcogenide materials is relatively easy, and many kinds of glasses have been prepared by means of melt quenching, vacuum depositions, and other less common methods such as spin coating and mechanical amorphization (Elliott, 1991; Popescu, 2000; Tanaka and Shimakawa, 2011; Adam and Zhang, 2014). Among the glasses, only selenium vitrifies as an elemental glass which is fairly stable at room temperature. Most of the stable binary glasses are compounds of a chalcogen atom and a group IV (14) or IV (15) atom, such as As(Ge)–S(Se,Te), where atomic ratios can widely be varied reflecting the covalency of atomic bonds. Ternary and more complicated glasses of various kinds have been prepared for some purposes (Popescu, 2000; Fairman and Ushkov, 2004; Adam and Zhang, 2014; Wang, 2014); these can probably be prepared by alloying with any kind of atom, including cations such as sodium and metallic atoms such as erbium, although the concentration may be limited. Oxychalcogenide and chalco-halide glasses can also be synthesized, and specifically, considerable interest has been paid for tellurite glasses such as TeO_2–P_2O_5 for photonics applications (Wang, 2014).

Thermal stability depends upon the glass. When heated, stable glasses such as As_2S_3 exhibit only the glass transition, some glasses such as selenium undergo glass transition and crystallization, and telluride glasses are likely to crystallize directly.

As shown by the horizontal sequence in **Figure 1** (Tanaka and Shimakawa, 2011), chalcogenide glasses tend to possess properties intermediate between those of organic polymers and oxide glasses, and **Table 1** compares physical properties of these three kinds of materials. Chalcogenide glasses are denser than polymers and oxide glasses, since they are composed of heavier

☆*Change History*: June 2015. K. Tanaka. (1) Three columns are added in Table 1. (2) In Figure 2, (a) is enlarged, (b) is slightly modified, and the captions are detailed. (3) In Figure 3, the captions are detailed. (4) Table 2 is modified. (5) In Table 3, a new column is added. (6) Figure 8 and related descriptions are newly added. (7) A new paragraph is added in Section 3. (8) In Section 4, two paragraphs are revised and a new figure, Figure 10, is added. (9) In Section 5, Figure 11 is added. (10) Old references are deleted, and new or frequently-cited ones are added.

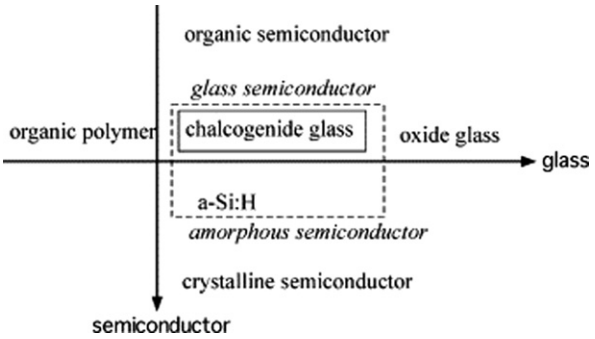

Figure 1 Characterization of chalcogenide glasses as glasses and semiconductors in comparison with other materials.

Table 1 Comparison of the density ρ, the bulk modulus B, the glass-transition temperature T_g, the thermal conductivity κ, the linear thermal-expansion coefficient β, the refractive index n, the optical gap E_g, and the vibrational threshold energy E_{vib} in polyethylene, As_2S_3, and SiO_2. The thermal conductivity of As_2S_3 scatters among reports

Material	ρ *(g cm^{-3})*	B *(10^{10} N m^{-2})*	T_g *(K)*	κ *(W m^{-1} K^{-1})*	β *(10^{-5} K^{-1})*	n	E_g *(eV)*	E_{vib} *(eV)*
Polyethylene	0.95	~0.2	150	0.4	15	1.46	5	0.4
As_2S_3	3.2	1.25	460	0.2–0.5	2.5	2.43	2.4	0.09
SiO_2	2.2	3.65	1450	1.4	0.055	1.46	8	0.3

elements (S, Se, Te) than those (H, C, Si, O) in the others. The constituent atoms also govern the region of optical transparency, which lies between the electronic gap E_g and the vibrational threshold E_{vib}.

Chalcogenide glasses bear some similarity to oxide glasses, since both oxygen and chalcogens belong to group VI (16) in the periodic table (Mott and Davis, 1979; Elliott, 1990; Tanaka and Shimakawa, 2011). The valence–electron configuration of all these elements is s^2p^4, in which two p-electrons form atomic bonds with two neighboring atoms (**Figures 2** and **3**). An exception is cation-chalcogenide glass, which will be mentioned later.

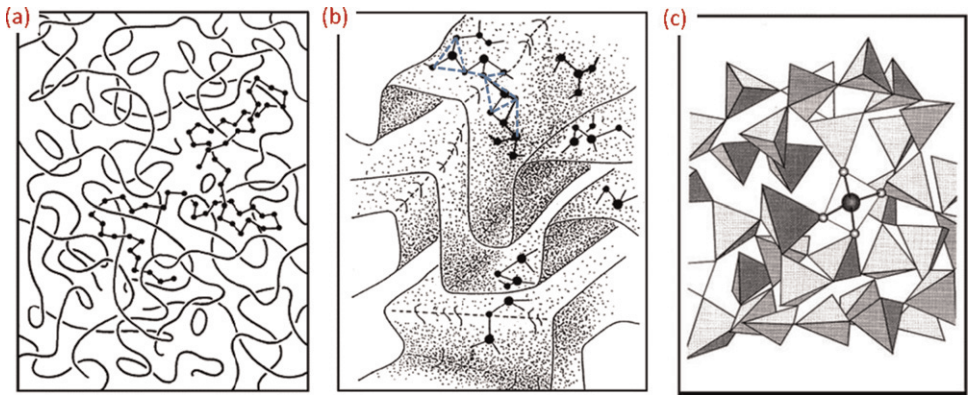

Figure 2 Illustrations of atomic structures in (a) Se, (b) $As_2S(Se)_3$, and (c) SiO_2. (a) Atoms are dotted only for one chain, may also contain ring molecules. (b) The three- and the two-fold coordinated circles represent As and S(Se) atoms, which form $AsS(Se)_{3/2}$ trigonal pyramids (dashed lines), which produce corner- and edge-shared connections and extend to distorted layer-like clusters. (c) The tetrahedra represent $SiO_{4/2}$ units, which are connected by the corners, producing three-dimensional continuous random networks. The bond length denoted by solid lines is typically 0.2–0.3 nm, and the intermolecular and interlayer distance in (a) and (b) is assumed to be 0.4–0.5 nm.

However, in more detail, there exist marked differences between chalcogenide and oxide glasses, among which the most essential may be the ionicity of atomic bonds. For instance, according to the Pauling's scale, As–Se and Si–O possess bond ionicities of 0.4 and 1.7. Taking the ionicity of Na–Cl of 2.1 into account, we can regard chalcogenide glasses as being covalent and oxides as ionic.

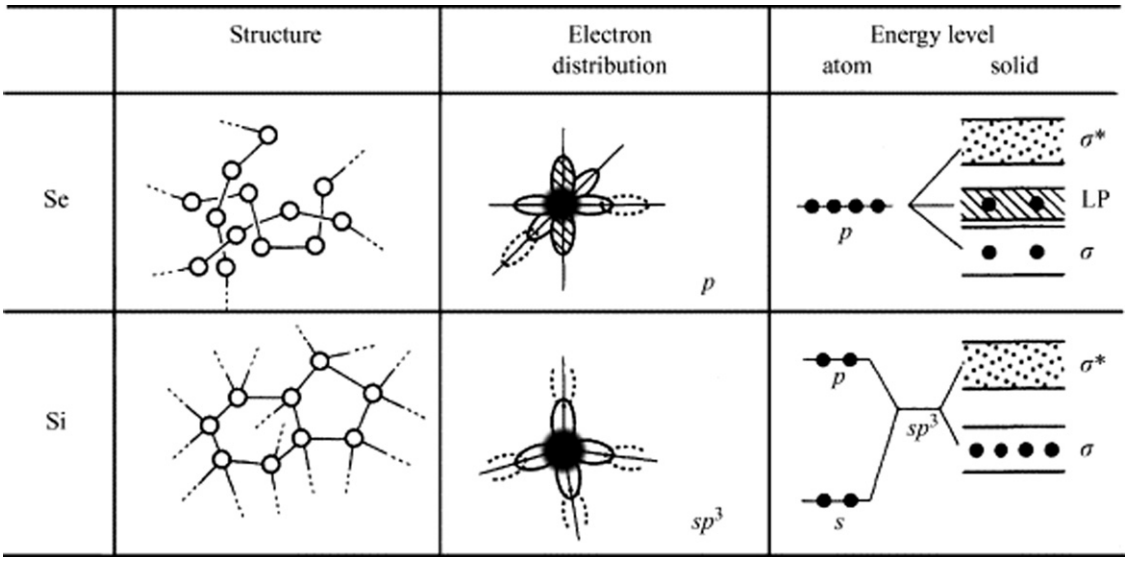

Figure 3 Comparison of a-Se and a-Si: the microscopic structure, the valence–electron distribution around an atom, and the electronic structures in an atom (left) and the solid (right). In Se, the bandgap appears between lone-pair (LP) and anti-bonding (σ^*) states, while in Si it exists between bonding (σ) and anti-bonding states of sp^3 hybrid orbitals.

The difference in the ionicity causes different bonding angles (Elliott, 1991; Tanaka and Shimakawa, 2011). In the chalcogenide glass, for example in As_2Se_3, As–Se–As forms an angle of about 100°, which seems to be governed by covalent *p*-electron orbitals (**Figure 3**). In contrast, in SiO_2 the Si–O–Si bond angle is distributed around 150°, which may be substantially influenced by Coulombic repulsive forces between positively charged silicon atoms. Hence, in As_2Se_3, $AsSe_{3/2}$ trigonal pyramids can be edge-shared (**Figure 2(a)**), while in SiO_2 only corner-sharing of $SiO_{4/2}$ tetrahedral units is permitted (**Figure 2(c)**). The coordination number, bond length, and bond angle specify the short-range structure up to the second-nearest neighbor atoms, which is nearly the same as that in the corresponding crystal.

The structure beyond the third-nearest neighbors, the so-called medium-range structure, remains controversial (Elliott, 1991; Singh and Shimakawa, 2003; Tanaka and Shimakawa, 2011; Salmon and Zeidler, 2015). This is because we have no experimental tools, which can provide direct information of the structure, and molecular dynamic simulations (Kolobov, 2003; Wang, 2014) face to some limitations in particle numbers, quenching rates, etc. There probably exist disorders in dihedral angles and small rings. In a wider scale, we may envisage distorted quasi-crystalline structures (**Figure 2(b)**), or otherwise, we may assume three-dimensional continuous random network structures, which were originally proposed for SiO_2 glass (**Figure 2(c)**). In other words, the former emphasizes a structural similarity to the corresponding crystal, and the latter a universality in glass structures.

However, for selenium, the structural controversy may be less serious (Elliott, 1991; Tanaka and Shimakawa, 2011). The material is assumed to be composed of entangled chains and/or ring molecules (**Figure 2(a)**), the ratio probably depending upon preparation conditions. Such one-dimensional structures are typical of organic polymers such as polyethylene and, because of this resemblance, a- (amorphous) Se can be referred to as an 'inorganic polymer.'

In covalent chalcogenide glasses, as illustrated in **Figure 4**, there exist some transitions of macroscopic properties at $\langle N\rangle = 2.4$ and 2.67 (Elliott, 1991; Phillips, 1999; Singh and Shimakawa, 2003; Tanaka and Shimakawa, 2011). Here, $\langle N\rangle$ is the average coordination number of atoms, which is defined as $\langle N\rangle = \Sigma x_i N_i$, where x_i is the atomic fraction ($\Sigma x_i = 1$) of constituent elements and N_i is the atomic coordination number, which is 2 for chalcogens (**Figures 2** and **3**).

A pioneering study by Phillips and Thorpe has interpreted the transition at 2.4 as follows (Phillips, 1999): In a glass with $\langle N\rangle < 2.4$, the structure is floppy, and there exist so-called zero-frequency vibrational modes. That is, supposing only the bond length and the bond angle provide structural constraints, there remain free (zero-frequency) vibrational modes. At the magic number $\langle N\rangle = 2.4$, which is derived from a simple constraint-counting formulation as $\langle N\rangle/2 + (2\langle N\rangle - 3) = 3$, the structure becomes just rigid, and stable glasses can be prepared. Above this point, the structure is over-constrained, and glass formation becomes difficult. This magic-number concept has successfully been applied also to oxide glasses such as $74SiO_2 \cdot 16Na_2O \cdot 10CaO$.

Further studies have demonstrated that the compositional dependence of some physical properties such as the density and the optical gap provides deeper insight (Phillips, 1999; Tanaka and Shimakawa, 2011). Tanaka has pointed out extrema and/or thresholds at $\langle N\rangle = 2.67$, which he interpreted as a signature of a topological phase transition from two-dimensional (< 2.67) to three-dimensional (> 2.67) structures, with the critical value being derived also simply as $\langle N\rangle/2 + (\langle N\rangle - 1) = 3$. As illustrated in **Figure 4**, however, some physical properties such as the glass-transition temperature increase monotonically with $\langle N\rangle$. Alter-

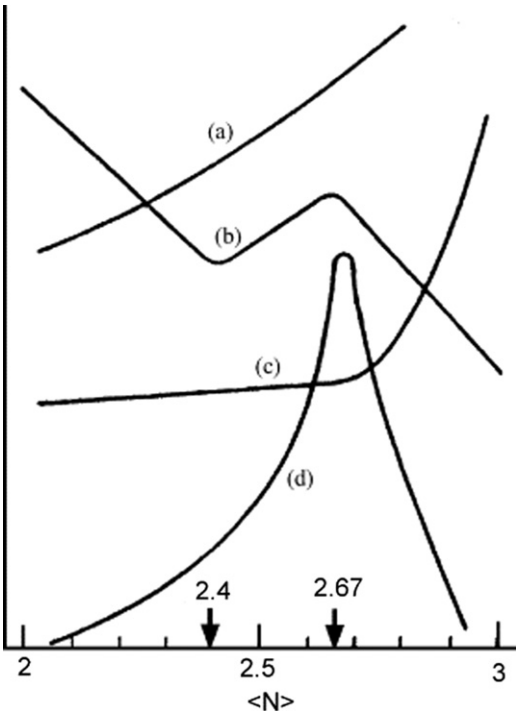

Figure 4 A schematic composition dependence of some properties as a function of the average coordination number $\langle N \rangle$. Examples are as follows: type (a) includes the position of the first-sharp X-ray diffraction peak and the glass-transition temperature; type (b), the bandgap energy, the specific volume, the specific heat, and the thermal expansion coefficient; type (c), the elastic constant and the density of tunneling states; and type (d), the intensity of the first sharp X-ray diffraction peak and the photodarkening effect.

natively, Boolchand insists the existence of intermediate phases for the structural transitions. It should be noted that such $\langle N \rangle$ dependence studies are inherent to covalent glasses, in which the *atomic* composition can be varied continuously.

On the other hand, with the vertical change in the periodic table from sulfur to selenium and tellurium, the atomic bond becomes more metallic (Borisova, 1981; Popescu, 2000; Tanaka and Shimakawa, 2011). Directional bonding character changes to fairly isotropic in telluride alloys, which are then likely to undergo crystallization relatively easily (see Section 4). The glass becomes darker in color, and the electrical conductivity becomes higher.

Chalcogenide glasses containing group I–III (1, 11, 12, 13) atoms are exceptional from the above descriptions (Borisova, 1981). These atoms are likely to behave as cations, which tend to add some specific features. For instance, in Cu–As–Se, it has been demonstrated that the coordination number of selenium increases from 2 to 4. It is also known that in the Cu–As–Se system, glass formation is possible along the line connecting As_2Se_3 and Cu_2Se. Such a glass-formation region has been interpreted by a formal valence shell model (Tanaka and Shimakawa, 2011), which assumes that lone-pair electrons are transferred to bonding states with compositional changes.

Another prominent feature, which should be pointed out here, is the ionic conduction in some glasses containing lithium, sodium, and silver (Borisova, 1981; Elliott, 1990; Fairman and Ushkov, 2004; Tanaka and Shimakawa, 2011; Adam and Zhang, 2014). In these glasses, the ion forms atomic bonds with chalcogen atoms with relatively long bond distances of 0.25–0.3 nm. This feature and the high dielectric constant ($\varepsilon_r \approx 10$) in chalcogenide glasses favor marked ionic conductivity, since Coulombic attractive forces are suppressed. Several glasses, such as Li_2S–P_2S_3–LiI, exhibit superionic conduction of 10^{-3} S cm^{-1} at room temperature. In contrast to the electronic conduction, which will be described in Section 2, the ionic conduction tends to be enhanced with structural disordering. For instance, the Ag^+ conductivities in crystalline and glassy $AgAsS_2$ are reported to be 10^{-7} and 10^{-6} S cm^{-1} (Tanaka and Miyamoto, 2015).

Finally, it should be noted that the atomic structure and related properties in chalcogenide glasses depend upon preparation procedures and history after preparation (Elliott, 1991; Tanaka and Shimakawa, 2011; Adam and Zhang, 2014). This prehistory dependence is common to all non-equilibrium systems, such as glass. For instance, as shown in **Figure 5**, Raman scattering spectra of As_2S_3 depend considerably upon the preparation methods.

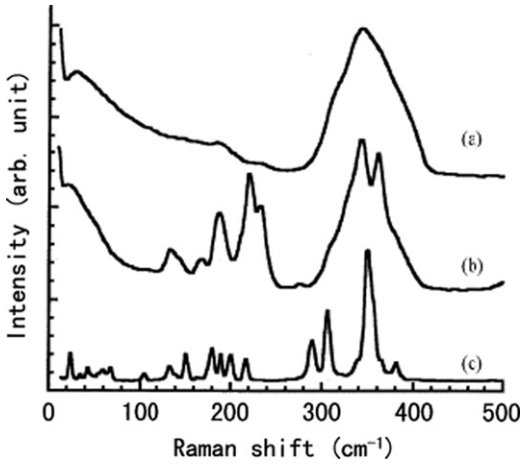

Figure 5 Raman scattering spectra of As_2S_3 in (a) a melt-quenched bulk glass and (b) an as-evaporated film, which are assumed to be networked and molecular, respectively. For comparison, a spectrum of the crystalline form is also shown in (c).

2 Electronic

Chalcogenide glasses possess electrical and optical bandgaps of 1–3 eV, and accordingly they can be regarded as amorphous semiconductors (Mott and Davis, 1979). The gap decreases in the sequence of sulfur, selenium, and tellurium, reflecting the enhanced metallic character. On the other hand, polyethylene and SiO_2 are insulators with optical gaps of 5–10 eV and vibrational edges at infrared wavelengths (**Table 1**), making these materials transparent at visible regions around $\sim$2.5 eV (**Figure 6**).

As a semiconductor, the overall property of chalcogenide glasses can be grasped as the vertical sequence in **Figure 1**. That is, with the change from organic semiconductors such as polyvinyl-carbazole, chalcogenides, hydrogenated amorphous silicon films, to crystalline semiconductors, the electronic mobility becomes higher, which can afford faster response in devices. The material also becomes more rigid. Instead, material prices seem to increase with this sequence, which may reflect their typical preparation methods, i.e., coating, evaporation, glow discharge, and crystal-growth techniques, respectively.

As exemplified in **Figure 3**, the electronic structure of a chalcogenide glass is essentially the same as that of the corresponding crystal (Mott and Davis, 1979; Elliott, 1990; Tanaka and Shimakawa, 2011). In chalcogenide glasses with the chalcogen coordination number of 2, the top of the valence band is composed of lone-pair *p*-electrons of chalcogen atoms, and the bottom of the conduction band is composed of anti-bonding states of covalent bonds. Since bandgap energy is governed by short-range structures, the value is normally similar ($\sim \pm 10\%$) to that in the corresponding crystal.

Due to this nature of the valence band, dramatic effects of pressure upon electronic properties appear (Elliott, 1991; Tanaka and Shimakawa, 2011). Hydrostatic compression preferentially contracts the intermolecular distance of $\sim$0.5 nm, and then the

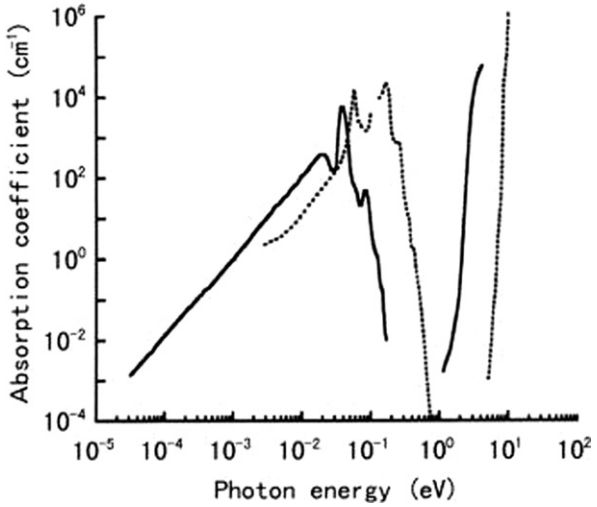

Figure 6 Optical absorption spectra of As_2S_3 (solid line) and SiO_2 (dotted line) glasses.

overlapping between lone-pair *p*-electrons is enhanced. As a result, the valence band broadens, and the bandgap remarkably decreases.

Optically, as shown in **Figure 6**, chalcogenide glasses are transparent between red (or near IR) and IR regions (Borisova, 1981; Elliott, 1991; Kokorina, 1996; Popescu, 2000; Adam and Zhang, 2014). The short-wavelength cutoff is determined by electronic excitation, and the long-wavelength limit by atomic vibrations (**Table 1**); this feature is common in semiconductors and insulators.

The electronic absorption edge consists of three spectral curves (Mott and Davis, 1979; Elliott, 1990; Singh and Shimakawa, 2003; Tanaka and Shimakawa, 2011). In the absorption region higher than $\sim 10^3$ cm^{-1}, the absorption spectrum $\alpha(h\nu)$ follows the functional dependence $(\alpha h\nu)^{1/2} \propto h\nu - E_g^{\ T}$ in many materials, and it is common to define the optical bandgap energy using $E_g^{\ T}$, the so-called Tauc gap. Note that the Tauc gap is lower than the mobility gap $E_g^{\ \mu}$, between extended states of the conduction-band bottom and the valence-band top, which may be evaluated from photoconduction spectra. For smaller absorption coefficients, a temperature-independent Urbach edge with the form $\alpha \propto \exp(h\nu/E_U)$ is observed, where E_U is the Urbach energy. Selenium is exceptional here, for which E_U is markedly temperature dependent. Interestingly, for chalcogenides $E_U \geq 50$ meV, which is comparable with $E_U \approx 50$ meV in hydrogenated amorphous silicon (Tanaka, 2014b). In the spectral region $\alpha \leq 10^0$ cm^{-1}, a weak absorption tail with a dependence of $\alpha \propto \exp(h\nu/E_W)$ is observed, where $E_W \approx 300$ meV in As_2S_3. This absorption tail is influenced by impurities, but even in purified samples the tail still exists. It may be due to intrinsic mid-gap states.

However, atomic structures responsible for the mid-gap states have been unable to be experimentally determined. Instead, the defect concept, including charged dangling bonds and/or valence alternation pairs, originally proposed by Mott and Street is repeatedly employed for the interpretation of many observations (Mott and Davis, 1979; Elliott, 1990; Fritzsche, 2000; Singh and Shimakawa, 2003). For instance, the photoluminescence, which is excited by photons with $h\nu \approx E_g$ and is emitted at $h\nu \approx E_g/2$, and photoinduced electron-spin signals at low temperatures have been interpreted as a manifestation of structural transformations of these defects. The density of such defects is estimated at $\sim 10^{17}$ cm^{-3} from estimated formation energy. However, there exist notable characteristic differences between Se and $As_2S(Se)_3$, which may be difficult to understand by the concept. Otherwise, some observations have been interpreted by assuming other defects such as wrong bonds (Elliott, 1991; Popescu, 2000; Tanaka and Shimakawa, 2011), i.e. homopolar bonds in stoichiometric compositions. Accordingly, it may be fair to assert that the defect structure remains controversial.

Electrically, glasses exhibit smaller conductivities than the corresponding crystals (Borisova, 1981; Elliott, 1990; Tanaka and Shimakawa, 2011). Specifically, sulfide glasses such as As_2S_3 and GeS_2 behave as genuine insulators, the conductivity σ $(=q\mu n)$ being smaller than 10^{-15} S cm^{-1}. This is because an effective carrier mobility μ is suppressed by band-tail and gap states, which are manifestations of disordered structures (Mott and Davis, 1979; Singh and Shimakawa, 2003). On the other hand, the carrier density n of intrinsic semiconductors is governed by the bandgap energy, and accordingly, the density is assumed to be similar to that in the corresponding crystal. In general, the position of the Fermi energy, which may be located near the center of the bandgap, cannot be controlled by impurity doping. It is mentioned here that a marked conductivity change between amorphous and crystalline states in Ge–Te films etc. is a hot topic in electrical phase-change devices (see Section 4).

In detail, the chalcogenide glass can be regarded as a *p*-type semiconductor or, more exactly, hole is more mobile than electrons (Elliott, 1991; Popescu, 2000; Tanaka and Shimakawa, 2011), which is contrastive to the opposite character in oxide glasses. The reason has not been elucidated. In selenium at room temperature, holes exhibit conventional Gaussian transport with a mobility of 0.1 cm^2(V s)$^{-1}$. However, at low temperatures and, in several materials, at room temperature, holes exhibit so-called dispersive transport, and the effective mobility decreases to 10^{-5} cm^2(V s)$^{-1}$ or even less. Such hole motions are described in terms of multiple trapping with band-tail states or hopping transport through gap states.

However, there are a few exceptions, such as Bi- and Pb-added selenides, in which the thermopower indicates *n*-type conduction (Elliott, 1991; Popescu, 2000; Tanaka and Shimakawa, 2011). In addition, Narushima *et al.* (2004) discovered a high *n*-type conductivity of 10^{-1} S cm^{-1} with a Hall mobility of 26 cm^2(V s)$^{-1}$ in amorphous $In_{49}S_{51}$ films. In these films, sulfur atoms seem to be fourfold coordinated, as in crystalline CdS, which is likely to cause the conductivity. Also, Hughes *et al.* (2014) have prepared *n*-type Bi–GeTe films through ion implantation.

Photoelectrical properties of chalcogenide glasses have been studied extensively (Mott and Davis, 1979; Popescu, 2000; Singh and Shimakawa, 2003; Fairman and Ushkov, 2004; Tanaka and Shimakawa, 2011), probably because of their unique photoconductive applications (see Section 4). Specifically, amorphous selenium films deposited onto substrates held at 50–60 °C are highly photoconductive, and the characteristics have been investigated extensively. Among many features examined, the one that is markedly different from that in conventional crystalline semiconductors is the existence of a 'non-photoconducting spectral gap'. As shown in **Figure 7**, the photoconductive spectral edges in amorphous selenium are blue-shifted by more than 0.5 eV from the optical absorption edge. Geminate recombination of photoexcited carriers, which suppresses photocurrents, is assumed to be responsible for the spectral gap. In addition, Juška and Arlaukas discovered 'avalanche multiplication' of photocreated carriers in amorphous selenium (Fairman and Ushkov, 2004; Tanaka and Shimakawa, 2011; Tanaka, 2014a). This phenomenon appears to be anomalous, since the disordered structure is assumed to be unfavorable for producing accelerated carriers, which can cause impact generation of other carriers.

Chalcogenide glasses are known to exhibit prominent nonlinear acoustic and optical effects (Kokorina, 1996; Tanaka and Shimakawa, 2011; Eggleton *et al.*, 2011; Adam and Zhang, 2014; Wang, 2014). **Table 2** compares some nonlinear parameters of

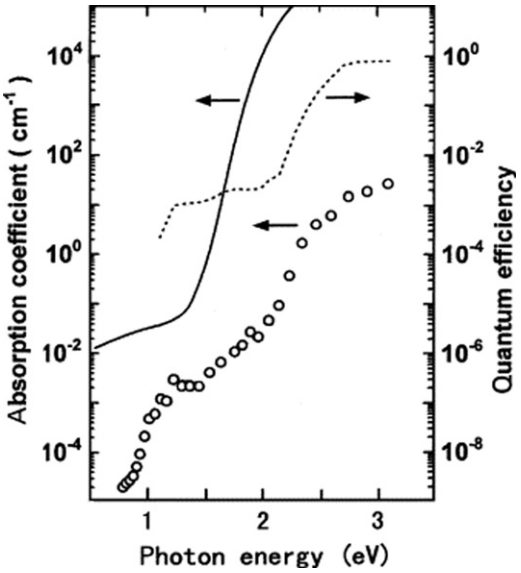

Figure 7 Comparison of some optical spectra for a-Se near the optical absorption edge. The solid line shows the optical absorption coefficient, the dotted line gives the photoconductive quantum efficiency, and the circles are the absorption coefficient derived from the constant-photocurrent method.

Table 2 Comparison of nonlinear coefficients and the refractive index n_0 in As_2S_3 and SiO_2 glasses. M_2 is the photoelastic figure of merit, M_a the nonlinear acoustic figure of merit, and n_2 the intensity-dependent refractive index

Material	M_2 *(10^{15} s^{-3} kg^{-1})*	M_a *(10^{-12} s^2 kg^{-1})*	n_2 *(10^{-16} cm^2 W^{-1})*	n_0
As_2S_3	433	240	200	2.43
SiO_2	1.5	0.4	2	1.46

As_2S_3 and SiO_2 glasses. It can be seen that As_2S_3 is more nonlinear than SiO_2 by a factor of 10^2. Among these parameters, the most promising may be the intensity-dependent refractive index n_2 (see Section 4), which modifies the refractive index n as $n = n_0 + n_2 I$, where n_0 is the conventional refractive index and I is light intensity. The greater n_2 in As_2S_3 than that in SiO_2 is consistent with a relation $n_2 \propto 1/E_g^4$, where E_g is the optical gap (Tanaka and Shimakawa, 2011).

3 Photoinduced Phenomena

After pioneering work of an optical phase-change phenomenon by Ovshinsky *et al.* around 1970, extensive studies have been made on photoinduced phenomena in chalcogenide glasses (Fritzsche, 2000; Popescu, 2000; Kolobov, 2003; Singh and Shimakawa, 2003; Tanaka and Shimakawa, 2011; Kolobov and Tominaga, 2012; Adam and Zhang, 2014). As shown in **Table 3**, the phenomena can be grouped into three categories: the photon mode, in which the photoelectronic excitation directly induces atomic structural changes; the photothermal mode, in which photoelectronic excitation induces some structural changes with the aid of thermal activation; and the heat mode, in which the temperature rise induced by optical absorption is essential (see Section 4). Interestingly, these three kinds of phenomena are likely to appear in sulfides, selenides, and tellurides, respectively. It is

Table 3 Typical optical gaps E_g and photoinduced phenomena appearing in oxide, sulfide, selenide, and telluride glasses

Material	E_g *(eV)*	*Photon*	*Photo-thermal*	*Heat*
Oxide	~6	Refractive-index increase		
Sulfide	2.5	Darkening, fluidity, shape change	Anisotropy, doping	
Selenide	2		Crystallization	
Telluride	1			Phase-change

also mentioned that oxide glasses such as Ge–SiO_2 undergo photoinduced refractive-index increases, which seem to originate from defect formation and densification.

The best-known heat-mode phenomenon is the optical phase change, or the so-called optical Ovonic effect (Kolobov, 2003; Kolobov and Tominaga, 2012; Adam and Zhang, 2014). This phenomenon appears in tellurium compounds, which undergo thermal crystallization. A light pulse heats the film sample above the crystallization temperature and, as a result, a transformation from amorphous to crystalline phases occurs. As illustrated in **Figure 8**, in some materials such as $Ge_2Sb_2Te_5$, this change is reversible. That is, a more intense light pulse heats the sample above the melting temperature, and a successive temperature quenching is able to reproduce the original amorphous structure. The optical phase change has widely been commercialized in optical memories (see Section 4), which triggers extensive studies on the mechanisms. For instance, why the crystallization occurs with time scales of ~ 10 ns is one of important problems, for which some researchers envisage leading roles of electronic processes (Kolobov, 2003).

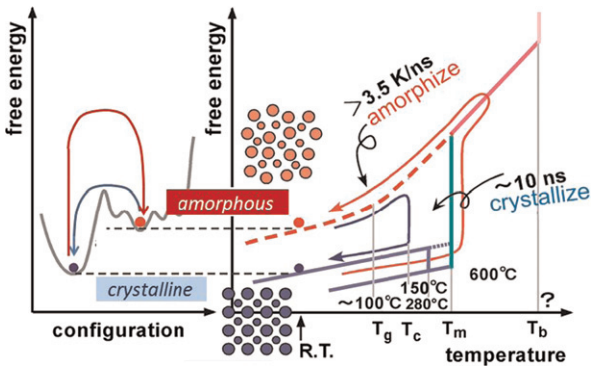

Figure 8 Principal features of the phase change in $Ge_2Sb_2Te_5$ between amorphous and crystalline states as functions of atomic configuration (left) and temperature (right). Note the existence of cubic and hexagonal crystalline phases, and the phase change occurs between amorphous and the cubic.

As for the photon-mode phenomena, reversible photodarkening and related changes have attracted considerable interest (Elliott, 1991; Fritzsche, 2000; Singh and Shimakawa, 2003; Kolobov, 2003; Tanaka and Shimakawa, 2011; Adam and Zhang, 2014). Here, light illumination induces a red-shift of the optical absorption edge, so that the sample becomes darker, while the red shift can be reversed with annealing at the glass-transition temperature. The refractive index in transparent wavelength regions increases with the red-shift, which is consistent with the expectation obtained from the Kramers–Krönig relation. Sample volume, and elastic and chemical properties also change with illumination and recover with annealing. As for the light, bandgap illumination ($h\nu \approx E_g$) has been assumed to be effective. However, studies demonstrate that sub-gap light with the photon energy lying in the Urbach-edge region also produces some changes, which can be more prominent than those induced by bandgap light. The photodarkening phenomenon appears only in covalent chalcogenide glasses, but by no means having been detected in the corresponding crystal and in oxide glasses. Some structural studies have demonstrated that the amorphous structure becomes more disordered with illumination. However, it is difficult to identify the structural change in amorphous networks, and accordingly, the mechanism remains indefinite.

More recently, dramatic phenomena such as photoinduced fluidity, giant volume expansion, and anisotropic deformations have been discovered in As(Ge)–S(Se) glasses (Tanaka and Shimakawa, 2011; Wang, 2014). It may be surprising that sample shapes change only by illumination of moderate-intensity light, which is unpolarized or linearly polarized. All these mechanical phenomena become more prominent under illumination at lower temperatures. The mechanisms are largely speculative, while it is plausible that photoexcited structural disordering and alignment through bond alternations are responsible for these phenomena.

An example of photothermal bulk phenomena is the photoinduced anisotropy (Fritzsche, 2000; Kolobov, 2003; Tanaka and Shimakawa, 2011). Macroscopically, untreated glasses are generally isotropic, while illumination with linearly polarized light can add some anisotropy such as dichroism, birefringence, and axial strains. Even unpolarized light can induce anisotropy if the light enters a sample from a side surface or with high incident angles. In addition, the anisotropic direction can be altered by illumination with other polarized light. Furthermore, the anisotropy can be erased by illumination with unpolarized or circularly polarized light or by annealing. However, at lower temperatures, the photoinduced anisotropy appears less efficient and, accordingly, this phenomenon can be understood to be induced by a photothermal process. Fritzsche (2000) has assumed the process that consists of directional changes of anisotropic structural elements, which exist in chalcogenide glasses. However, the atomic structure of the elements is vague. It should be mentioned here that in some materials, such as amorphous selenium, oriented crystals can be produced by illumination with polarized light.

So-called photodoping, which was discovered by Kostyshin and co-workers, is a famous photothermal chemical reaction (**Figure 9**; Fritzsche, 2000; Kolobov, 2003; Tanaka and Shimakawa, 2011). Consider a bilayer structure consisting of silver and AsS_2 films. When this bilayer is exposed to light, the silver film dissolves rapidly into the AsS_2. For instance, if the silver film is 10 nm in thickness, and the exposure is provided from the semitransparent silver side using a 100 W ultrahigh-pressure mercury lamp, the silver film will dissolve within a few minutes. Since the reaction becomes slower if the sample is illuminated at lower temperatures, this can be regarded as a photothermal phenomenon. However, it should be mentioned that temperature rise induced by illumination is not essential.

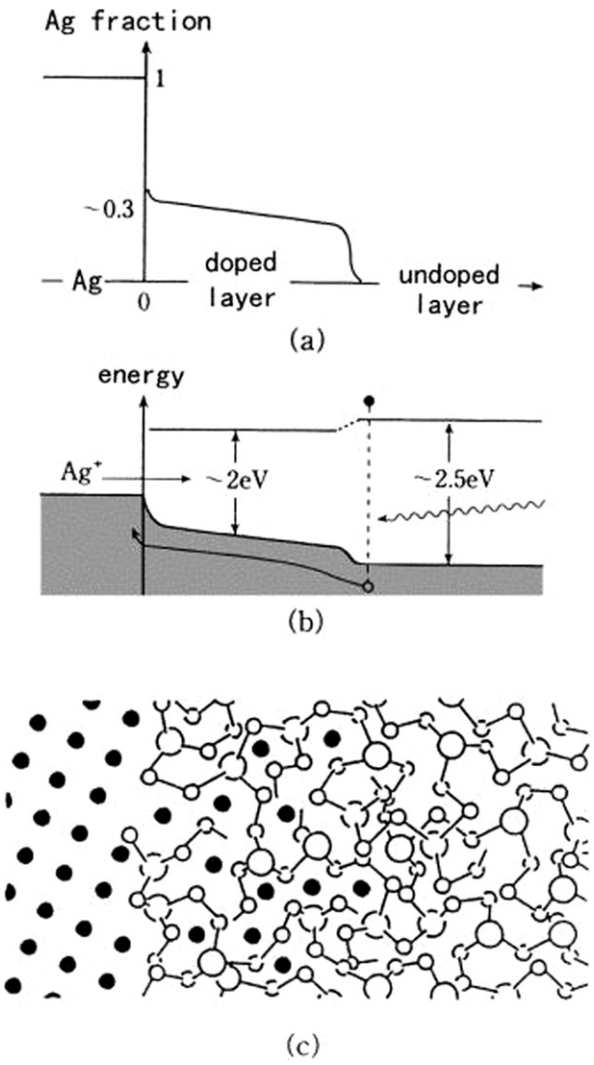

Figure 9 Schematic illustrations of a model for photodoping in an Ag:AsS_2 system when the photodoping is progressing. (a) The Ag atomic concentration, (b) the band diagram, where electron, hole, and Ag^+ motions are illustrated, and (c) the microscopic structure.

Much work has been done in order to understand the mechanism of this dramatic phenomenon (Popescu, 2000; Kolobov, 2003; Adam and Zhang, 2014). Owen has proposed that the reaction $Ag + AsS_2 \rightarrow AgAsS_2$ is favored thermodynamically and, accordingly, the composition of the photodoped layer becomes $AgAsS_2$. Note that, due to the reaction, AsS_2 is preferred to As_2S_3. The driving force causing the silver dissolution seems to be provided by photoexcited hole motions. As for applications, the photodoping has been demonstrated to be promising as a lithographic process, having an ultrahigh spatial resolution of about 10 nm. However, practical usages seem to remain.

In addition to the phenomena described here, there are also several irreversible and transitory changes. Examples are photopolymerization and opto-mechanical effects. The reader may refer to Fritzsche (2000), Popescu (2000), Kolobov (2003), and Tanaka and Shimakawa (2011).

Finally, it should be mentioned that not only photons but also other excitations such as electrons and γ-rays can give rise to a variety of structural changes (Popescu, 2000; Fairman and Ushkov, 2004; Adam and Zhang, 2014; Wang, 2014). Some of these are similar to, but others are dissimilar from, the corresponding photon effects. For instance, electron beams can enhance silver doping into chalcogenide films like photons, while the beam can suppress crystallization of selenium, in contrast to the photo-crystallization phenomenon. It should also be mentioned that studies using scanning tunneling microscopes etc. demonstrate nanometer-scale structural changes in chalcogenide glasses (Tanaka and Shimakawa, 2011).

4 Applications

Four kinds of applications are commercially available or practically utilized. These rely upon the unique features of chalcogenide glasses: meta-stability, efficient photoconductivity, infrared transparency, and ionic conduction.

The most profitable may be the phase-change phenomenon (see Section 3) (Elliott, 1991; Tanaka and Shimakawa, 2011; Kolobov and Tominaga, 2012; Adam and Zhang, 2014). It has been applied to erasable high-density optical memories, the so-called Digital Versatile Disk (DVD) system, in which pulsed light emitted from a blue laser diode is focused upon crystalline $Ge_2Sb_2Te_5$ films, converting the region to an amorphous bit through rapid quenching, which is read as reflectivity difference with intensity-reduced light. The bit size, which is determined by a diffraction-limited light spot, has been reduced to $\sim$100 nm, giving a memory capacity of 100 GB in triple-layer disks (Yamada, 2012). The phase change can also be induced electrically. In the device so-called Phase-Change Random Access Memory (PC-RAM), nano-meter scale telluride dots are phase-changed by joule heats, and the amorphous-crystalline states are read through electric resistance. The crystallization time could be shortened to sub-ps scales (Loke *et al.*, 2012). Commercial devices now seem to be in intense developing stages, facing severe competition with other next-generation electrical memories such as ferroelectric RAMs (Wong *et al.*, 2010; Fujisaki, 2013).

The second category is photoconductive applications (Popescu, 2000; Tanaka and Shimakawa, 2011). As known, wide usages of a-Se films as photoreceptors in copying machines (Mott and Davis, 1979; Elliott, 1991) had been taken place by organic photoconductors, while new applications of the material are growing. In photoconductive targets in vidicons, avalanche multiplication in a-Se films (see Section 2) is employed for detecting optical images with ultrahigh sensitivity; higher more than 100 times than that obtained by the conventional crystalline Si devices. As shown in **Figure 10**, the vidicon is now combined with field-emitter arrays and becomes compact with a thickness of 1 cm (Honda *et al.*, 2015). On the other hand, in X-ray detecting flat panels (Singh and Shimakawa, 2003, Tanaka and Shimakawa, 2011), a-Se films with a typical size of 40×40 cm^2 and a thickness of 0.5–1 mm are employed to convert X-ray images to electric currents, with spatial resolutions of $\sim$0.1 mm (Kasap *et al.*, 2011). This application owes to a heavy atomic number ($=34$) of selenium and high X-ray conductive gains in the insulating amorphous film.

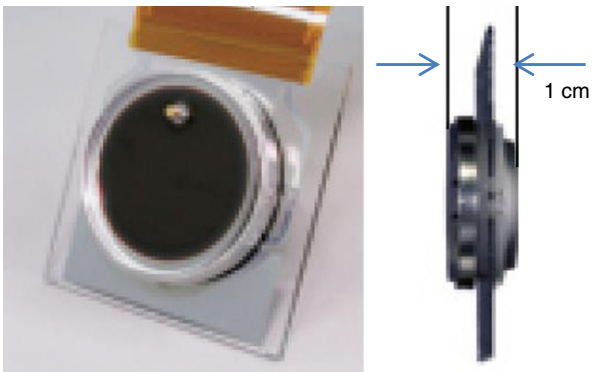

Figure 10 Photograph of a Field-Emitter Array – High-gain Avalanche Rushing amorphous Photoconductor (FEA-HARP) (Modified from N. Egami, Oyo Butsuri 78 (2009) 343).

The third application is purely optical (Kokorina, 1996; Elliott, 1990; Popescu, 2000; Fairman and Ushkov, 2004; Tanaka and Shimakawa, 2011; Adam and Zhang, 2014; Wang, 2014). Since the chalcogenide glass is transparent in IR regions, it has been utilized for IR optical components such as lenses and windows. It can also be utilized through purification and drawing to prepare IR-transmitting optical fibers, which are utilized for highly sensitive IR spectroscopy. Fibers can also be employed as a matrix incorporating rare-earth ions, for example Er^{3+}, which are promising for preparing functional devices such as optical amplifiers. Planar, channeled, and photonic-structure waveguides have also been explored, in which photoinduced phenomena (Section 3) are frequently harnessed to shape tuning (Kolobov, 2003). In addition, high nonlinearity (Section 2) is combined with these fibers

and waveguides, giving rise to optical devices including all-optical switches, supercontinuum generators, Raman amplifiers, and so forth (Eggleton *et al.*, 2011).

Lastly, chalcogenide glasses containing group I (1 and 11) elements such as silver are used as highly sensitive ionic sensors (Popescu, 2000; Fairman and Ushkov, 2004). Some lithium-containing glasses and ceramics, e.g. $Li_2S–P_2S_5$, can also be utilized as electrolytes in all-solid-state batteries (Adam and Zhang, 2014), which may have promising future.

5 Final Remarks

Chalcogenide glasses can be regarded as glassy semiconductors, and the level of our present understanding can be summarized as follows. For the atomic structural components, listed at the left-hand side in **Figure 11**, we have obtained relatively firm knowledge of the short-range structure, which covers the coordination number, the bond length, and the bond angle. Also, dependence on atomic compositions, which are practically possible only in covalent glasses, has added valuable insights into the chalcogenide-glass science. Now, the problem is shifting to the identification of medium-range structures, density fluctuations, and defects. For these structures, however, there are few effective experimental techniques available at present. In addition, the quasi-stability, which is an inherent character to glasses, also makes the problem intricate. Under such situations, we may employ computer simulations and/or refine simple structural models which can interpret as many observations as possible. It may be fair to say that, at the present stage, because of the incomplete structural knowledge, the chalcogenide-glass science is far behind the one constructed for single crystalline semiconductors.

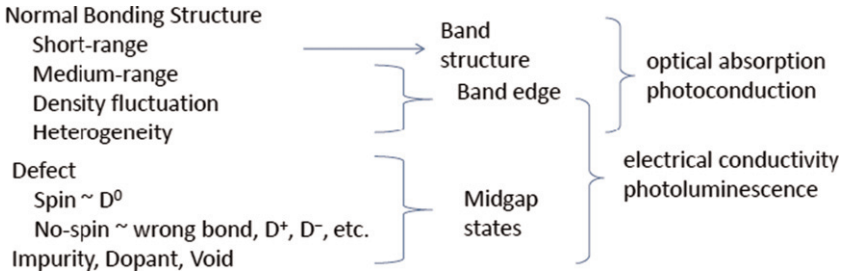

Figure 11 Relationship between microscopic structures (left), electronic states (center), and electronic properties (right). 'D' represents dangling bonds, which may include valence alternation pairs.

Many problems, fundamental and simple, remain unresolved. For instance, the glass transition may be a common problem and also the biggest problem in glass science. On the other hand, electronic behaviors near the band edge and in the bandgap are also important problems both fundamentally and in applications. For instance, no one can give a convincing answer to such a simple question as "Why in chalcogenide glasses are holes more mobile than electrons?" Answering to such questions will pave the way to further developments of amorphous semiconductor sciences and unique functional devices.

References

Adam, J.L., Zhang, X. (Eds.), 2014. Chalcogenide Glasses. Oxford: Woodhead Publishing.
Borisova, Z.U., 1981. Glassy Semiconductors. New York: Plenum.
Eggleton, B.J., Luther-Davies, B., Richardson, K., 2011. Chalcogenide photonics. Nat. Photon. 5, 141–148.
Elliott, S.R., 1990. Physics of Amorphous Materials, second ed. Essex: Longman Scientific & Technical.
Elliott, S.R., 1991. Chalcogenide glasses. In: Zarzycki, J. (Ed.), Materials Science and Technology. New York: VCH, pp. 375–454.
Fairman, R., Ushkov, B. (Eds.), 2004. Semiconducting Chalcogenide Glass I, II, & III. Amsterdam: Elsevier.
Fritzsche, H., 2000. Light induced effects in glasses. In: Boolchand, P. (Ed.), Insulating and Semiconducting Glasses. Singapore: World Scientific (Chapter 10).
Fujisaki, Y., 2013. Review of emerging new solid-state non-volatile memories. Jpn. J. Appl. Phys. 52, 040001.
Honda, Y., Nanba, M., Miyakawa, K., Kubota, M., Egami, N., 2015. Active-matrix Spindt-type field emitter array with faster response time for image sensor with high-gain avalanche rushing amorphous photoconductor target. J. Vac. Sci. Technol. B 33, 012205.
Hughes, M.A., Fedorenko, Y., Gholipour, B., *et al.*, 2014. n-Type chalcogenides by ion implantation. Nat. Commun. 5, 5346.
Kasap, S., Frey, J.B., Belev, G., *et al.*, 2011. Amorphous and polycrystalline photoconductors for direct conversion flat panel x-ray image sensors. Sensors 11, 5112–5157.
Kokorina, V.F., 1996. Glasses for Infrared Optic. Boca Raton, FL: CRC Press.
Kolobov, A.V. (Ed.), 2003. Photo-Induced Metastability in Amorphous Semiconductors. Weinheim: Wiley-VCH.
Kolobov, A., Tominaga, J., 2012. Chalcogenides: Metastability and Phase Change Phenomena. Berlin: Springer-Verlag.
Loke, D., Lee, T.H., Wang, W.J., *et al.*, 2012. Breaking the speed limits of phase-change memory. Science 336, 1566–1569.
Mott, N.F., Davis, E.A., 1979. Electronic Processes in Non-Crystalline Materials, second ed. Oxford: Clarendon Press. 1979.
Narushima, S., Hiroki, M., Ueda, K., *et al.*, 2004. Electrical properties and local structure of n-type conducting amorphous indium sulphide. Philos. Mag. Lett. 84, 665–671.
Phillips, J.C., 1999. Constraint theory and stiffness percolation in network glasses. In: Thorpe, M., Duxbury, P.M. (Eds.), Rigidity Theory and Applications. Dordrecht, The Netherlands: Kluwer, p. 155.

Popescu, M.A., 2000. Non-Crystalline Chalcogenides. Dordrecht: Kluwer Academic Publishers.
Salmon, P.S., Zeidler, A., 2015. Networks under pressure: The development of *in situ* high-pressure neutron diffraction for glassy and liquid materials. J. Phys.: Condens. Matter 27, 133201.
Singh, J., Shimakawa, K., 2003. Advances in Amorphous Semiconductors. London: Taylor & Francis.
Tanaka, K., 2014a. Avalanche breakdown in amorphous selenium (a-Se) and related materials: brief review, critique, and proposal. J. Optoelectron. Adv. Mater. 16, 243–251.
Tanaka, K., 2014b. Minimal Urbach energy in non-crystalline materials. J. Non-Cryst. Solids 389, 35–37.
Tanaka, K., Miyamoto, Y., 2015. Ionic conductivities in crystalline, glassy, and liquid $AgAsS_2$. Solid State Ion. 269, 106–109.
Tanaka, K., Shimakawa, K., 2011. Amorphous Chalcogenide Semiconductors and Related Materials. New York: Springer.
Wang, R. (Ed.), 2014. Amorphous Chalcogenides: Advances and Applications. Singapore: Pan Stanford Publishing.
Wong, H.-S.P., Raoux, S., Kim, S.B., *et al*., 2010. Phase change memory. Proc. IEEE 98, 2201–2227.
Yamada, N., 2012. Origin, secret, and application of the ideal phase-change material GeSbTe. Phys. Status Solidi B 249, 1837–1842.